Journal of
Water & Climate Change

IWA PUBLISHING

Journal of Water and Climate Change Vol 12 No 8, 3714 doi: 10.2166/wcc.2021.171

Study on the driven mechanism of hydrologic drought based on the lithology-combined structure of the Karst drainage basin in South China

Zhonghua He[a,*], Hong Liang[a] and Zhaohui Yang[b]

[a] School of Geographic and Environment Science, Guizhou Normal University, Guiyang, Guizhou 550001, China
[b] Department of Emergency Management of Guizhou Province, Ministry of Emergency Management of the People's Republic of China, Guiyang, Guizhou 550001, China
*Corresponding author. E-mail: hezhonghua7621@126.com

ABSTRACT

Hydrologic drought, considered as a typical natural phenomenon in the background of global climate changes, is the continuation and development of meteorological and agricultural droughts, and is the ultimate and most thoroughly drought. The research area controlled by the 55 hydrological sections in South China is selected in this paper, and the intensity and frequency of hydrologic droughts are analyzed by the Standardized Runoff Index (*SRI*), and the driven mechanism of watershed lithologies to hydrologic droughts is discussed. The results show that (i) the hydrological drought of Karst drainage basins is shown the *gradual aggravation* from the west to east parts in South China, with the significant *north–south stripe* distributions at the *SRI_3* and *SRI_6*; (ii) the occurring probability of hydrological droughts is the *Limestone-type Karst Basin* (II and III, 0.17) < *Dolomite-type Karst Basin* (I and IV, 0.22) < *Non-Karst Basin* (V, 0.25) in terms of combination types of basin lithologies, and (iii) the *Karst Basin* (I and III, 0.18) < *Semi-Karst Basin* (II and IV, 0.2) < *Non-Karst Basin* (V, 0.25) in terms of basin lithologies. Therefore, this proves that the most water-stored spaces are found in Karst Basins under the differential dissolution or erosion effects of soluble water, followed by in the Semi-Karst Basin, the least water-stored spaces in the Non-Karst Basin.

Key words: driven mechanism, hydrologic drought, Karst drainage basin, South China

HIGHLIGHTS

- We explored the driving mechanism of watershed lithologic composite structures to hydrologic droughts.
- It is 'gradually aggravated' with the distribution of 'north–south stripe' for the hydrologic droughts from west to east in the Karst drainage basins in South China.
- The order of drought occurrence probability is the Karst Drainage Basin of Limestone Type < Karst Drainage Basin of Dolomite Type < Non-Karst Drainage Basin.

1. INTRODUCTION

Hydrologic drought, considered as a typical natural phenomenon in the background of global climate changes, is the continuation and development of meteorological and agricultural droughts, and is the ultimate and most thoroughly drought (Kang & Guo 1991). The drought cannot be simply attributed to the climate anomalies and precipitation reduction under the special and fragile Karst ecological environments, but to the water storage capacity of underlying surface media shown as the lithology, landform, soil, vegetation, etc. The watershed lithology is one of important medium factors, and their functions are mainly shown that (i) for the different types of watershed lithologies, there are different kinds of watershed landforms developed in Karst basins, which will lead to the different runoff characteristics on the surface and underground, and affect the watershed storage capacity (Liang 1995, 1997; Liang & Wang 1998); (ii) the different soil structures and vegetation types are developed due to different types of watershed lithologies with different anti-weathering abilities and weathering crust thicknesses formed in Karst basins, and they influence the infiltration and runoff of rainfall on the surface and underground, which results in the different watershed storage capacity; and (iii) for the different types of watershed lithologies, with the different mechanical properties and the different development intensities and scales of bedrock fissures, are developed the different water-stored spaces or drainage channels in Karst basins, which affects the watershed storage capacity. For example, Liang (1995) discussed the flood peak effects caused by the coupling differences between the different spatio-temporal scales

of Karst drainage basins and the different spatial configurations of landform types. It found that there is a positive proportional relationship between peak values and watershed areas in the Non-Karst basins, and a special relationship in the middle and small Karst basins due to the double geomorphic system structures on the surface and underground. Meanwhile, the watershed lithology is one of the important factors affecting the low-flow runoff moduli in the middle and small Karst basins. For instance, the larger the proportion of watershed limestones, the smaller the low-flow runoff moduli, and the larger the proportion of watershed dolomites, the larger the low-flow runoff moduli (Liang & Wang 1998). Wang's research (Wang *et al.* 2002) showed that the impacts of different natural factors on the low-flow runoff in the dry seasons, such as the spatial scales of Karst basins, watershed lithologies, and landform types, are very significant. For instance, the larger the proportion of peak-cluster depressions, the smaller the low-flow runoff moduli, and the larger the proportion of the Fenglin Rongyuan (Basin), the larger the low-flow runoff moduli. Therefore, to make the identification and extraction of lithologic types in Karst drainage basins, and to analyze their spatial coupling structures in this paper, it is helpful to study the rule of watershed water storage, and to reveal the driven mechanism of watershed hydrologic droughts (Liang 1995, 1997; Liang & Wang 1998). For the previous studies on hydrological droughts, some scholars have carried out the quantitative expressions for the hydrologic drought characteristics by the theory of runs (Yevjevich 1967) and have studied the extreme hydrologic drought characteristics obeyed the normal, lognormal, and gamma distributions (Sen 1977, 1990, 1991; Guven 1983; Sharma 1998). The Regional Drought Area Index (*RDAI*) and the Drought Potential Index (*DPI*) are used to characterize regional hydrological droughts (Fleig *et al.* 2011), and the relationship between the drought duration and intensity was also further discussed by Kim & Valdés (2006) and Panu & Sharma (2009). The influences of river regulation and water diversion from other places on the process and level of hydrologic droughts are analyzed by Wen *et al.* (2011) employing the Standardized Runoff Index (*SRI*) and the Standardized Precipitation Index (*SPI*). The level, process, and recurrence period of hydrologic droughts are studied by the Palmer Drought Severity Index (*PDSI*), the Soil Moisture Model (*SMM*), and the Standardized Rainfall Index (*SRI*), as well as the Vegetation Health Index (*VHI*) (Nyabeze 2004; Mondal & Mujumdar 2015), respectively. The time-series analysis and random simulation of hydrologic drought severities have been carried out using an autoregression model (Abebe & Foerch 2008), and the probabilistic prediction of hydrologic droughts is analyzed by Hao *et al.* (2016) using a conditional probability based on the meta-Gaussian model. Seibert *et al.* (2017) made the seasonal forecast for hydrologic droughts using a statistical analysis method in the Limpopo Basin. In addition, Rudd *et al.* (2017) firstly characterized droughts over the last century by a national-scale gridded hydrologic model well-simulated low flow in many catchments across Great Britain. The historic drought periods (1891–2015) were better identified employing time series of monthly mean river flow and soil moisture based on the threshold level method. Meanwhile, the spatial–temporal distribution differences between the meteorological and hydrological droughts are explored by some scholars (Hisdal & Tallaksen 2003; Tallaksen *et al.* 2009; Yang *et al.* 2021) in terms of basin scales. The temporal and spatial evolution patterns of hydrological droughts are studied by employing different drought indexes in terms of the national or regional scales. For example, the hydrological drought severity in region of Thessaly, Greece with varying geomorphologic characteristics are explored by Vasiliades & Loukas (2009) using the Palmer four indices (PDSI, Weighted PDSI, PHDI, and the moisture anomaly *Z*-index) combined with the UTHBAL conceptual water balance model. Tabari *et al.* (2013) discussed the hydrological drought characteristics by the Streamflow Drought Index (*SDI*) in the northwest of Iran over the period 1975–2009. It was found that some of the streamflow volume series did not follow the normal distribution, and extreme droughts occurred most frequently in the last 12 years from 1997–1998 to 2008–2009. Leng *et al.* (2015) assessed the climate change impact in China on droughts from meteorological, agricultural, and hydrologic perspectives by the *SPI*, *SSWI*, and *SRI*, respectively. They thought that the meteorological, hydrological, and agricultural droughts will become more severe, prolonged, and frequent in 2020–2049 compared with 1971–2000. Vazifehkhah & Kahya (2018) analyzed the influences of winter North Atlantic Oscillation (NAO) and Arctic Oscillation (AO) extreme phases on hydrological drought using a Standardized Streamflow Index (*SSI*) over Turkey and northern Iran. The droughts in various magnitudes during the positive extreme phases of NAO were found in Western and Eastern Turkey while fewer droughts were observed in Iran during the negative NAO and AO extreme phases. The hydrological droughts were more strongly affected by the negative NAO and AO extreme phases in a shorter period than by the positive NAO and AO phases in a longer period. Ding *et al.* (2021) studied the propagation relationship between meteorological and hydrological drought, and the most susceptible regions in China and global scale. There was a stronger relationship between the two types of drought in summer and autumn than in spring and winter. The most susceptible regions were tropical and subtropical Chinese southern zones in China and equatorial and warm temperate climate zones in global. The variable threshold level approach is employed to analyze the hydrological drought

characteristics in Bundelkhand region of Central India during 1974–2009 (Swetalina & Thomas 2016) and to estimate the return period of hydrologic droughts in southeastern semi-arid region of Iran. It was found that the vegetation cover play important roles in the hydrologic drought length (Modarres & Sarhadi 2010). Drought duration, severity, and frequency are analyzed for steep topography in the central Vietnam and other parts of Southeast Asia at different timescales (Firoz *et al.* 2018). The more severe droughts are observed in groundwater dependent areas, where have longer durations rather than higher intensities (Rudd *et al.* 2017). The relationship between the El Niño-Southern Oscillation (ENSO) and hydrologic variability in the United States is discussed using Empirical Orthogonal Function (EOF)/Principal Component Analysis (PCA), and it is found the positive relationships in the Pacific Northwest, whereas negative relationships in southern California and the northern Great Plains (Ryu *et al.* 2010). Finally, to explore the feasibility of the *SRI* in Southwest China, Liu *et al.* (2016) simulated a long-term daily hydrological and meteorological data series by the Xinanjiang model and calculated the *SRI*. It proves that the onset, severity, and duration of extremely droughts are detected well by the *SRI*. For the studies on hydrological droughts in China, Feng & Wang (1997) and Feng & Jia (1997) mainly discussed the influence factors of runoff volume in the dry season, and the identification method of hydrological droughts based on the theory of runs, and analyzed the hydrologic drought severities by the time fractal dimensions. Feng (1993, 1994, 1995) studied the probability density and distribution functions of extreme hydrologic drought durations. The joint distribution of hydrologic drought characteristics is constructed employing the Copula Joint Distribution Function (Yan *et al.* 2007; Ma & Song 2010; Xu *et al.* 2010; Zhou *et al.* 2011). However, most of the researches are mainly to make the identification, characteristic analysis, and prediction for hydrologic droughts by different drought indices, respectively. For instance, Zhai *et al.* (2015) established a new hydrologic drought assessment index such as Standard Water Resources Index (*SWRI*) and developed a complete basic framework of hydrologic drought identification, assessment, and characteristic analysis combined with the distributed hydrologic model, the copula function, and the statistical test method. The Standardized Streamflow Drought Index (*SSDI*) is established based on the optimal distributions such as the logistic, normal, two-parameter lognormal, or Weibull probability distribution (Zhao & Zhao 2016), and it is validated in the applicability and rationality in the Fenhe River Basin. Combined with the percentages of runoff anomaly and precipitation anomaly, Wu *et al.* (2016) constructed the Regional Hydrological Drought Index (*RHDI*) and obtained the corresponding frequency of drought grade, and further determined the threshold value of the different drought levels for regional hydrological droughts. The Copula Model of two-variable joint distribution of hydrologic drought characteristics is built based on the test method of Cramer–von Mises Statistics associated with Rosenblatt transfer (Tu *et al.* 2016), and it is analyzed the hydrologic drought characteristics and water shortage responses in the Dongjiang River Basin under a changing environment. Ren *et al.* (2016) quantitatively separated the contribution of climate change and human activities on runoff reduction based on the Variable Infiltration Capacity Model (*VICM*) and analyzed the spatio-temporal evolution characteristics of hydrological droughts by the *SRI*. The Standard Precipitation Evapotranspiration Index (*SPEI*) and the *SDI* are used to analyze the evaluation characteristics of both meteorological and hydrologic droughts and to discuss the response of hydrologic droughts to meteorological droughts (Li *et al.* 2016). The *SRI*, *SDI*, and associated indicators with the trend, time lag cross-correlation are applied to analyze the spatial–temporal characteristics of meteorological and hydrologic droughts across the Yellow River Basin (YRB) during the periods 1961–2010 (He *et al.* 2015a). According to the correlation characteristics of seasonal runoff, the copula prediction model of hydrologic droughts based on the copula function, runoff distribution function, and *SRI* is constructed by Zhang *et al.* (2016), and the empirical analysis is carried out by the hydrologic station of the Aksu River West Bride.

However, the present studies on the hydrologic droughts in Karst basins, except for some relevant research contents of this team (He & Chen 2013; He *et al.* 2013, 2014, 2015b, 2018a, 2018b), have not seen more detailed studies reporting. Thus, the objectives of this study are (i) to discuss the types of Karst drainage basins based on the spatial coupling structures of different lithologies in Section 4.1; (ii) to comparatively analyze the hydrological drought characteristics in terms of different time scales and spatial coupling of lithologies in Section 4.2; and (iii) to systematically study the driven mechanism of the single lithology and the different lithologies coupled to hydrological droughts in Section 4.3. Therefore, it is beneficial to promote the development of Karst hydrographic geomorphology.

2. STUDY AREAS

The South China (SC), taking Guizhou, Yunnan, and Guangxi as the center, is a typical distribution region of the Cone Karst, Sword Karst, and Tower Karst. This study was to select the Karst drainage basins controlled by 55 hydrological stations in the SC as the research area. It is enclosed by the eastern longitudes of 101°55′55″–110°55′45″ and northern latitudes of 22°

42′57″–29°13′11″ with an area of 352,526 km^2 and an average elevation of 1,065.62 m. The research area is mainly included the most area of Guizhou Province (37.97%), southeastern area of Yunnan Province (25.36%), and northwestern and northern areas of Guangxi Province (36.67%) (Figure 1). It is located in the climatic zones of north subtropical humid climate and south subtropical semi-humid climate with the mean annual rainfall of 1,000–1,300 mm, and the average annual temperature of 16–23 °C. The study area is divided into two parts of the Yangtze and Pearl River Basins by the Wumeng–Miaoling Mountains. That means the Jinshajiang River System, the Upper Yangtze River Mainstream System, the Wujiang River System, and the Dongting Lake System of the Yangtze River Basin are located in the north of research area, whereas the Duliu River System (in Guizhou), the Yuanjiang River System (in Yunnan), and the Xijiang River System (in Guangxi) of the Pearl River Basin in the south of research area.

3. DATA AND METHODS

3.1. Research data

3.1.1. Hydrologic data

Hydrologic drought is usually shown by the reduction and the cutoff of the runoff volumes on the surface and underground rivers, and the decline of table levels in the lakes and reservoirs (Van Loon & Van Lanen 2012; Van Loon & Laaha 2015). Hydrologic data of the 55 hydrological stations (including 25 in Guizhou, 19 in Guangxi, and 11 in Yunnan; Table 1) in this study were obtained from the *Hydrology Statistical Yearbook* compiled by the Ministry of Water Resources of the People's Republic of China (Hydrologic Year Book of People's Republic of China[1]) and calculated the monthly average runoff volume during the periods 1970–2013. The hydrological stations selected in this paper must have 44 years of continuous hydrological observation, and continuous defect data must be less than 3 months. All the data will be made quality analysis (reliability, homogeneity, and representativeness), and for the months of defect data are interpolated by the cubic spline function. The interpolations must keep the same change trend as the total values during the periods 1970–2013. In order to eliminate the influence of different basin areas, hydrologic data were standardized in this study.

3.1.2. Lithologic data

Firstly, we all know that the geological lithological types and structures are basically unchanged during the periods 1970–2013, because the formation and evolution of geologic lithologies are a slow geological process. This paper made some preprocessing for TM images corresponding to the mean runoff of the minimum month in 2006 (Time: January to December 2006) and extracted the study area of remote sensing images controlled by 55 hydrological stations (He *et al.* 2012). Secondly, the research area was extracted from the *Comprehensive Geological Map of 1:500,000 in Guizhou, Yunnan, and Guangxi Provinces* carried out by the geometric correction and projection correction, which was fused with the TM images. Thirdly, the remote sensing information of watershed lithologies was automatically extracted using object-oriented classification technology based on the *Comprehensive Geological Map of 1:500,000 in Guizhou, Yunnan, and Guangxi Provinces* (Jiao & Liang 2002). Finally, to make the statistics for the lithologic types of areas and to calculate the area percentages (Table 1).

3.2. Research methods

3.2.1. Identification of hydrological drought

Hydrologic drought is a phenomenon when the river flow is lower than its normal value. In other words, the river flow cannot satisfy the water supply demand in a certain period (Van Loon & Van Lanen 2012; Van Loon & Laaha 2015). According to the definition of hydrological droughts and Karst basin characteristics (Tsakiris *et al.* 2007; Liu *et al.* 2012; López-Moreno *et al.* 2013; Jehanzaib *et al.* 2020; Zhou *et al.* 2020), the *SRI* was quoted to describe the hydrological drought characteristics in this paper. The *SRI* can be expressed as follows:

$$SRI_{i,k} = \begin{cases} -\left(t - \dfrac{c_0 + c_1 t + c_2 t^2}{1 + d_1 t + d_2 t^2 + d_3 t^3}\right), & \text{for } 0 < H_{i,k}(x) \le 0.5 \\ \left(t - \dfrac{c_0 + c_1 t + c_2 t^2}{1 + d_1 t + d_2 t^2 + d_3 t^3}\right), & \text{for } 0.5 < H_{i,k}(x) \le 1.0 \end{cases} \quad (1)$$

[1] Hydrologic Year Book of People's Republic of China *Hydrologic Data of Yangtze River Basin*, Volume 6 and *Hydrologic Data of Pearl River Basin*, Volume 8.

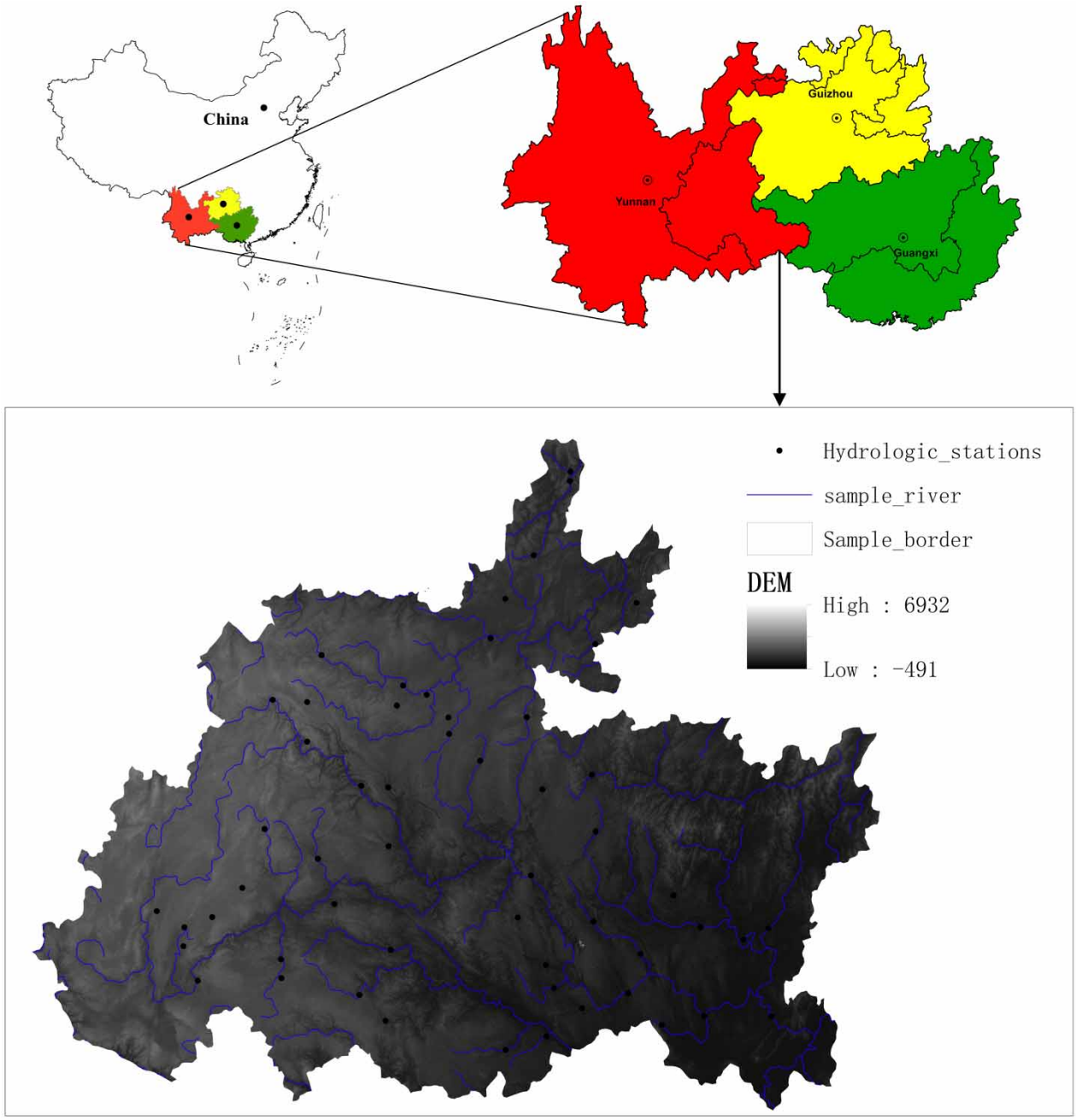

Figure 1 | Distribution diagram of the research areas.

where

$$t = \sqrt{\ln\left(\frac{1}{(H_{i,k}(X)^2)}\right)}, \quad \text{for } 0 < H_{i,k}(x) \leq 0.5$$

$$t = \sqrt{\ln\left(\frac{1}{1.0 - (H_{i,k}(X)^2)}\right)}, \quad \text{for } 0.5 < H_{i,k}(x) \leq 1.0$$

Table 1 | The area percentage of basin lithologic types (%)

Lithology																
No.	Station	River	C	D	ε	J	K	O	P	Pt	S	T	Z	Longitude (E)	Latitude (N)	Elevation (m)	Area (km^2)
1	Wujiayuanzi	Mei Jiang	21.41	0	9.34	0.59	0	23.89	0	0	16.59	28.18	0	107°41′	28°54′	814.86	1,230
2	Qixingguan	Liuchong River	8.53	0.62	0.28	1.08	0	0.33	58.38	0	0.31	30.49	0	104°57′	27°09′	1,718.35	2,999
3	Tatian River (two)	Tatian River	10.98	6.01	0	0.83	0	0	60.28	0	0.09	21.81	0	105°40′	25°17′	1,262.02	1,391
4	Zhangba	Furong River	6.91	0	23.03	0.64	0	31.62	9.33	0	22.97	5.49	0	107°41′	28°48′	788.75	5,454
5	Gaoche	Dabang River	4.67	0	0	0.21	0.25	0	17.17	0	0	77.71	0	105°42′	25°50′	1,184.9	2,264
6	Panjiangqiao (three)	Beipan River	15.55	2.91	0.11	0.96	0.02	0	54.56	0	0	25.88	0	105°23′	25°51′	1,571.1	14,350
7	Xiawan	Dumu River	14.71	52.1	0.33	0	0	3.06	19.7	0	4.29	5.81	0	107°10′	26°32′	1,123.19	1,433
8	Huishui	Lian Jiang	20.88	21.1	0	0.46	2.35	0	28.64	0	0	26.57	0	106°36′	26°07′	1,107.43	908
9	Wujiangdu (three)	Wujiang River	3.86	0.05	7.93	1.61	0.21	0.74	30.12	0.17	0	54.79	0.52	106°47′	27°18′	1,255.16	27,838
10	Xiangjiang	Xiangjiang River	0	0	44.76	0.73	0	8.3	7.62	0	1.57	21.98	15.03	106°56′	27°41′	930.1	559
11	Libo	Zhang Jiang	58.35	1.34	0	0	0	0	28.52	0	0	11.79	0	107°53′	25°24′	776.2	1,213
12	Zhijin	Zhijin River	0	0	0	0	0	0	100	0	0	0	0	105°46′	26°40′	1,397.79	66.4
13	Hongjiadu (two)	Liuchong River	1.64	0	2.38	3.37	0	1.16	35.5	0	0	55.35	0.59	105°52′	26°52′	1,439.45	9,656
14	Yuqing (three)	Yuqing River	0	0	34.85	0	15.26	0.13	1.76	28.77	0	0.17	19.06	107°54′	27°14′	769.35	610
15	Yangchang	Sancha River	16.65	1.43	0	0	0.15	0	63.11	0	0.06	18.61	0	105°11′	26°39′	1,881.45	2,696
16	Huangmaocun (two)	Yangchang River	1.13	0.46	0	0.25	3.41	0	15.18	0	0	79.58	0	106°20′	26°23′	1,301.52	793
17	Maiweng (two)	Taohuayuan River	0	0	0	0	0	0	70.49	0	0	29.51	0	106°19′	26°32′	1,275.36	62
18	Pinghu	Liudong River	47.39	20.24	0	0	0	0	18.03	0	0	14.33	0	107°19′	25°50′	928.79	1,441
19	Maling (two)	Mabie River	3.25	0	0	0	0	0	19.88	0	0	76.87	0	104°55′	25°12′	1,502.93	2,277
20	Xiaozhai	Kedu River	21.21	0.32	0	1.01	0	0	50.7	0	0	26.76	0	104°32′	26°36′	1,948.11	2,082
21	Yachihe (three)	Wujiang River	3.97	0.09	2.15	1.6	0.19	0.57	39.91	0	0	51.2	0.32	106°09′	26°51′	1,369.64	18,180
22	Baben	Duliu River	7.1	64.52	3.98	0	0	9.98	1.58	0	12.57	0.29	0	107°52′	26°00′	713.64	1,439
23	Shiqian	Shiqian River	0	0	32.4	0	0	23.41	6.31	1.45	31.24	4.1	1.09	108°14′	27°32′	742.34	723
24	Dadukou	Beipan River	10.72	6.08	0	0.85	0	0	59.98	0	0.09	22.28	0	104°48′	26°19′	1,903.51	8,454
25	Wangcao	Furong River	5.33	0	14.54	0	0	22.09	12.78	0	4.91	40.34	0	107°16′	28°05′	831.9	413
26	Bailin	Lingqi River	16.24	8.1	0	0	0.66	0	20.87	0	0	54.13	0	107°22′	23°55′	541.73	1,714
27	Douan	Hongshui River	35.88	10.31	0	0.73	0.93	0	20.35	0	0	31.81	0	108°11′	25°35′	393.21	119,245
28	Ronghua	Jianhe	24.54	21.45	0.94	0	0	0	11.71	0	0	41.35	0	106°53′	23°20′	725.87	1,880

(*Continued.*)

Table 1 | Continued

Lithology																
No.	Station	River	C	D	ε	J	K	O	P	Pt	S	T	Z	Longitude (E)	Latitude (N)	Elevation (m)	Area (km^2)
29	Yingzhu	Yingzhu River	6.31	11.5	1.12	3.76	0	0.11	7.67	2.71	0	66.82	0	107°19′	23°27′	601.88	26,936
30	Malong (three)	Diao Jiang	52.48	12.42	0	0.43	0	0	22.97	0	0	11.7	0	108°19′	24°14′	352.31	2,814
31	Wuxuan (two)	Qian Jiang	24.19	35.56	37.82	0	0	0	2.43	0	0	0	0	109°39′	23°35′	108.04	1,722
32	Donggan	Donggan River	34.79	14.42	1.03	0.4	7.15	8.27	23.24	0	0	10.69	0	108°30′	23°33′	123.69	3,829
33	Dingan (three)	Tuoniang River	10.15	6.88	1.77	0	0	0	0	5.2	0	76	0	105°42′	24°18′	900.46	4,424
34	Fengshan (two)	Panyang River	18.26	11.02	0	0	0	0	12.34	0	0	58.38	0	107°02′	24°32′	570.26	370
35	Qianjiang	Hongshui River	38.82	10.51	0.15	0.42	1.39	1.16	24.06	0	0	23.49	0	108°28′	23°37′	315.27	128,165
36	Liuzhou (two)	Rong Jiang	18.47	9.67	8.42	0.13	8.15	1.08	3.76	24.07	0.52	0.84	24.9	109°24′	24°20′	365.41	45,785
37	Tiane	Hongshui River	11.44	6.13	1.5	0.35	0.18	0.01	20.25	7.41	0.7	51.89	0.13	107°09′	25°00′	1,343.35	105,830
38	Hekou	Diao Jiang	44.71	24.46	0	1.18	0	0	10.63	0	0	19.02	0	107°50′	24°33′	453.63	1,045
39	Duiting	Luoqing River	17.26	76.55	5.5	0	0.68	0	0	0	0	0	0	109°41′	24°26′	182.89	6,705
40	Sancha	Long Jiang	9.68	6.37	12.05	0.2	0.22	0.98	0.42	35.3	0	0	34.78	108°57′	24°28′	369.33	15,870
41	Tianhe	Dongxiao River	12.57	7.21	1.55	0.29	0.1	0.01	19.9	7.25	0.68	50.34	0.08	108°41′	24°47′	380.6	735
42	Cifu	Panyang River	15.35	7.48	0	0	0.61	0	20.9	0	0	55.66	0	107°19′	24°08′	380.6	2,262
43	Fengwu	Pingzhi River	37.96	24.75	0	0	0	0	7	0	0	30.3	0	107°42′	23°43′	324.01	894
44	Gupeng	Gupeng River	48.59	4.55	0	0	0	0	36.1	0	0	10.76	0	108°36′	23°51′	320	316
45	Hebian	Kuaize River	0.82	13.47	0	0	0	0	75.22	0	0	10.49	0	104°21′	25°28′	1,536	1,973.87
46	Yiguba	Yinhong River	0	0	0	0	0	0	0	0	0	100	0	103°49′	24°38′	254	1,854.68
47	Funing	Putting River	11.01	46.68	23.08	0	0	5.78	6.92	0.65	0	5.88	0	105°37′	23°37′	3,972	1,200.55
48	Xiyangjie	Xiyang River	25.2	21.67	6.2	0	0	0	0	2.51	0	44.42	0	105°20′	23°53′	2,649	1,334.1
49	Huangjiazhuang	Bajiang	17.59	20.27	15.32	0	0	0	30.14	9.82	6.86	0	0	103°13′	24°41′	440	1,854.8
50	Youjiazhai	Dianxi River	7.71	51.81	0	0	0	0	16.1	5.47	0	16.14	2.77	103°26′	24°23′	1,856	1,771.13
51	Dayubu	Baima River	10.62	66.55	0	0	0	0	6.41	16.42	0	0	0	103°31′	24°30′	424	1,951
52	Jiangbianjie (two)	Nanpan River	6.7	26.24	11.16	0.6	0.03	0	15.93	30.67	4.89	3.25	0.52	103°37′	24°01′	25,116	1,701.62
53	Gelei	Qingshui River	33.16	4.37	0.19	0	0	0	1.24	2.3	0	58.74	0	104°31′	24°05′	3,186	1,530.37
54	Qingshui River	Qingshui River	29.18	3.79	0.15	0	0	0	2.69	3.66	0	60.54	0	104°31′	24°15′	4,156	1,476.6
55	Tagu	Xijiuxi River	34.38	6.8	0	0	0	0	23.96	0.95	0	33.91	0	104°08′	24°54′	1,910	1,924.47

Notes: C represents limestone with dolomitic limestone. D represents carbon shale with sandstone. ε represents limestone and dolomite in the upper part of the basin, dolomite in the lower part, and quartz sandstone in the bottom. J represents limestone with mud limestone and shale. K represents thick block sandstone with mudstone. O represents thick limestone with dolomite. P represents medium thickness limestone with breccia dolomite and siliceous limestone. Pt represents sericite slate with siltstone in the upper part of the basin, and siltstone with sericite slate in the bottom. S represents grayish green shale, sandy shale with sandstone, and quartz sandstone in the upper part of the basin, and purple shale, sandy shale in the bottom. T represents dolomite, mud dolomite with mudstone. Z represents dolomite with silicon strip dolomite in the upper part of the basin, and mud dolomite in the bottom.

$c_0 = 2.515517$, $c_1 = 0.802853$, $c_2 = 0.010328$, $d_1 = 1.432788$, $d_2 = 0.189269$, and $d_3 = 0.001308$.

$$H_{i,k}(x) = q_{i,k} + (1 - q_{i,k})F_{i,k}(x) \tag{2}$$

in which q is the probability of zero precipitation and $F_{i,k}(x)$ is the cumulative probability of the gamma distribution.

$$F_{i,k}(x) = \int_0^x f(x_{i,j})dx_{i,j} \tag{3}$$

$$f(x_{i,j}) = \frac{1}{\beta_{i,k}^{\gamma_{i,k}}\Gamma(\gamma_{i,k})} x_{i,j}^{\gamma_{i,k}-1} e^{\frac{-x_{i,j}}{\beta_{i,k}}}, \quad \text{for} > 0 \tag{4}$$

in which $\gamma_{i,k}$ and $\beta_{i,k}$ are the shape and scale parameters, respectively, and $\Gamma(\gamma_{i,k})$ is the gamma function.

$$\gamma_{i,k} = \frac{1}{4A_{i,k}}\left(1 + \sqrt{1 + \frac{4A_{i,k}}{3}}\right), \quad \beta_{i,k} = \frac{\bar{x}_{i,j}}{\gamma_{i,k}}$$

in which $A_{i,k} = \ln(\bar{x}_{i,j}) - \left(\frac{\sum \ln(x_{i,j})}{N_{i,k}}\right)$.

$$X_{i,j} = \sum_{j=1}^{3k} Q_{i,j}, \quad i = 1, 2, \ldots, \; j = 1, 2, \ldots, \; k = 1, 2, 3, 4 \tag{5}$$

where $Q_{i,j}$ refers to the accumulated runoff volume of the jth month in the ith hydrologic year, and $X_{i,j}$ denotes the accumulated runoff volume of the kth reference period in the ith hydrologic year. $k = 1, 2, 3, 4$ means October to December, October to March, October to June, and October to September, respectively (Nalbantis & Tsakiris 2009; Tigkas *et al.* 2012; Tabari *et al.* 2013).

A positive *SRI* means humid, whereas a negative *SRI* means drought. Moreover, when *SRI* is negative, the larger the absolute value of the *SRIs* means the serious hydrological drought. According to *SRI*, hydrological droughts can be divided into five levels, namely the Non-Drought for the $1.0 \le SRI \le 3.0$, the Mild Drought for the $-0.99 \le SRI \le 0.99$, the Moderate Drought for the $-1.49 \le SRI \le -1.0$, the Severe Drought for the $-1.99 \le SRI \le -1.5$, and the Extreme Drought for the $-3.0 \le SRI \le -2.0$ (Table 2) (Nalbantis & Tsakiris 2009; Wen *et al.* 2011; Jehanzaib *et al.* 2020).

3.2.2. Analysis of hydrologic drought mechanism

According to the definition of the Bayesian formula (Liao *et al.* 2007), to assume the independent random events (n) $B_1, B_2, \ldots, B_n$ are satisfied with the $B_i \cap B_j = \Phi$ $(i \neq j)$ (Φ represents impossible event), and $P\left(\bigcup_{i=1}^{n}\right) = 1$, $P(B_i) > 0$ $(i = 1, 2, \ldots, n)$. For any event A ($P(A) > 0$), there is:

$$P(B_k|A) = \frac{P(B_k)P(A|B_k)}{\sum_{k=1}^{c} P(B_k)P(A|B_k)} \tag{6}$$

where $P(B_k)$ refers to the hypothesis probability before the test, and $P(B_k|A)$ refers to the probability after the test.

Table 2 | Drought classification based on the *SRI* value and the corresponding cumulative probability

Drought Grade	Category	*SRI* Values	Cumulative Probability
1	Non-Drought	1.0 to 3.0	0.8413–0.9986
2	Mild Drought	−0.99 to 0.99	0.1587–0.8413
3	Moderate Drought	−1.49 to −1.0	0.0668–0.1587
4	Severe Drought	−1.99 to −1.5	0.0228–0.0668
5	Extreme Drought	−3.0 to −2.0	0.0014–0.0228

This paper supposed that $X = (x_{ij})_{m\times n}$ is the information matrix of lithological types in the research areas, and $Y = (y_i)_{m\times 1}$ is the drought level matrix of hydrologic droughts. In which x_{ij} is the area percentage of the jth type of lithologies, the ith level of hydrologic droughts, and y_i is the area percentage of the ith level of hydrologic droughts.

To presume that B_i represents the hydrologic drought event y_i affected by the jth type of lithology x_{ij}. Therefore, the uncertainty of hydrological droughts can be described by the conditional probability $P(y_i|x_{ij})$. The conditional probability $P(y_i|x_{ij})$ is expressed as:

$$P(y_i|x_{ij}) = \frac{P(y_i)P(x_{ij}|y_i)}{\sum_{i=1}^{5} P(y_i)P(x_{ij}|y_i)} \tag{7}$$

In a maximum likelihood classification, the maximum value of $\{P(y_i|x_{ij}),\ i = 1, 2, \ldots, 5\}$ will be selected, if there is $P(B_i|x_{ij}) > P(B_r|x_{ij})$, for all $i \neq r$. Namely, the hydrological drought is belonged to the category B_i. It is called the probability vector for all probability values $P(B_i|x_{ij})$ of the impact of each lithologic type index on hydrologic drought levels, which will be used to describe the uncertainty of lithological type indicators.

4. RESULTS AND ANALYSIS

4.1. Analysis of the watershed lithology-combined structure

As shown in Table 1, the watershed lithologies, without a single type, are mainly mixed with two or more than types of lithologies in Karst drainage basins. Therefore, to make the classification for the watershed sample areas by the system clustering method based on the watershed lithology-combined characteristics, and to draw the cluster pedigree by the SPSS software (Figure 2).

It can be seen that there are certain similarities between different basins in the cluster pedigree chart. The watershed lithological types could be divided into five types of combining structures according to the marking distance equal to 20 (Wang *et al.* 2002).

Class I (c26, c42, c34, c5, c19, c46, c16, c37, c41, c33, c13, c21, c9, c29): The largest (65%) is the area percentage of the dolomites, mud dolomite with mudstone (T), followed by the medium thickness limestones with breccia dolomite and siliceous limestone (P) with the area percentage 19%, and the smallest (1%) is the area percentage of the limestones and dolomites in the upper part of the basins, dolomite in the lower part, and quartz sandstone in the bottom (ε). Therefore, the basin with the lithology-combined structures is called a *Dolomite-type Karst Basin*.

Class II (c6, c20, c3, c24, c2, c12, c45, c17, c15): The largest (66%) is the area percentage (66%) of medium thickness limestones with breccia dolomite and siliceous limestone (P), followed by the dolomite, mud dolomite with mudstone (T) with the area percentage 21%, and the smallest (3%) is the area percentage of limestones with mud limestone and shale (J), and carbon shale with sandstone (D). Therefore, the basin with the lithology-combined structures is called a *Limestone-type Semi-Karst Basin*.

Class III (c53, c54, c28, c43, c48, c8, c32, c11, c44, c18, c30, c55, c27, c35, c38): The largest (38%) is the area percentage of limestones with dolomitic limestone (C), followed by the dolomite, mud dolomite with mudstone (T) with the area percentage 29%, and the smallest (1%) is the area percentage of thick block sandstones with mudstone (K). Therefore, the basin with the lithology-combined structures is called a *Limestone-type Karst Basin*.

Class IV (c1, c4, c23, c25, c31, c47, c10): The largest (26%) is the area percentage of limestones and dolomites in the upper part of the basin, dolomite in the lower part, and quartz sandstone in the bottom (ε), followed by the thick limestones with dolomite (O) with the area percentage 16%, and the smallest (2%) is the area percentage of dolomites with silicon strip dolomite in the upper part of the basin, and mud dolomite in the bottom (Z). Therefore, the basin with the lithology-combined structures is called a *Dolomite-type Semi-Karst Basin*.

Class V (c14, c36, c40, c49, c52, c50, c51, c7, c39, c22): The largest (27.85%) is the area percentage of carbon shales with sandstone (D), followed by the sericite slates with siltstone in the upper part of the basin, and siltstones with sericite slate in the bottom (Pt) with the area percentage 15%, and the smallest (2%) is the area percentage of thick limestones with dolomite (O). Therefore, the basin with the lithology-combined structures is called a *Non-Karst Basin*.

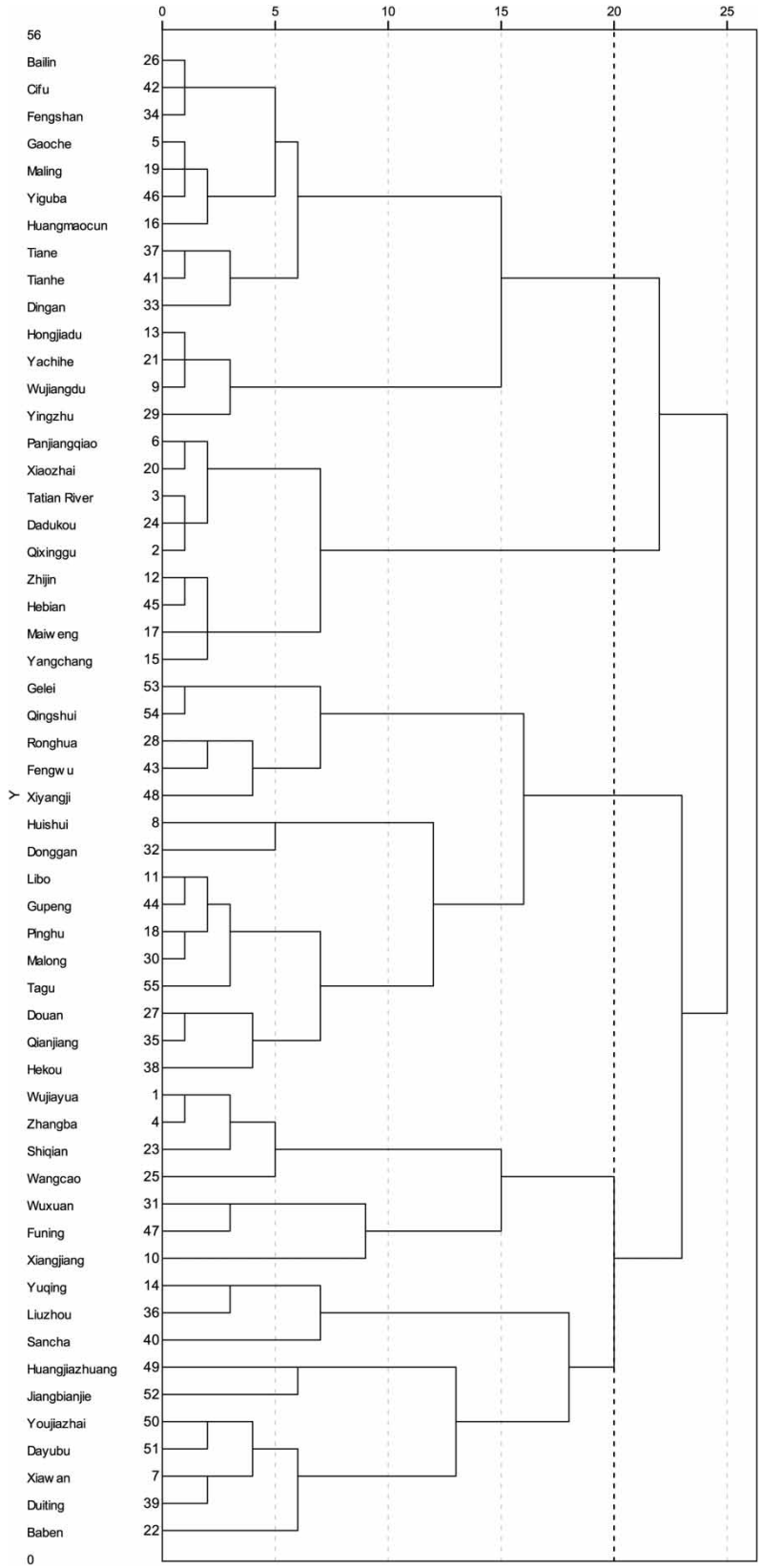

Figure 2 | The cluster pedigree chart of drainage basins.

4.2. Analysis of watershed hydrologic drought

4.2.1. Analysis of hydrological drought characteristics at different time scales

Hydrological drought characteristics in South China at the different time scales (*SRI_3*, *SRI_6*, *SRI_9*, and *SRI_12*) (SC) were calculated based on the data of monthly mean runoff during the periods 1970–2013 by the *SRI* in this study (Figure 3).

In terms of the temporal evolution of hydrologic droughts, (i) the distribution areas of hydrological droughts in the Karst drainage basins of South China are larger, and drought intensities are shown a decreasing trend. Among them, the hydrological droughts at the *SRI_3*, *SRI_6*, and *SRI_9* are relatively serious with the area percentages of 98.99, 99.63, and 98.46%, respectively, and relatively lighter at the *SRI_12* with the area percentage of 77.43% (Figure 3(d)). It means that the hydrological drought areas in Karst basins are gradually decreasing with the increase of time scales. (ii) The distribution areas of moderate hydrological droughts at the *SRI_3* and *SRI_6* are the largest with the area percentages of 43.23 and 52.26% shown in Figure 3(a) and 3(b), respectively, followed by the mild hydrologic droughts with the area percentages of 27.74 and 20.12%, and the smallest the Non-Drought. It indicates that the runoff regulation functions of Karst drainage basins are weaker or nonsignificant with the time scales decreasing. While the distribution areas of mild hydrological droughts at the *SRI_9* and *SRI_12* are the largest (62.19 and 66.21%), followed by the moderate hydrological drought (27.32%) at the *SRI_9*, the Non-Drought (22.57%) at the *SRI_12*, and the smallest the Non-Drought at the *SRI_9*, the severe hydrologic droughts at the *SRI_12* (Figure 3(c) and 3(d)). (iii) For the severe or above droughts, the largest are the drought areas at the *SRI_3* and *SRI_6* with the area percentages of 25.04 and 27.28%, followed by the *SRI_9* (8.97%), and the smallest (6.57%) at the *SRI_12* in Figure 3(d). This means that the drought areas of the severe or above hydrologic droughts are

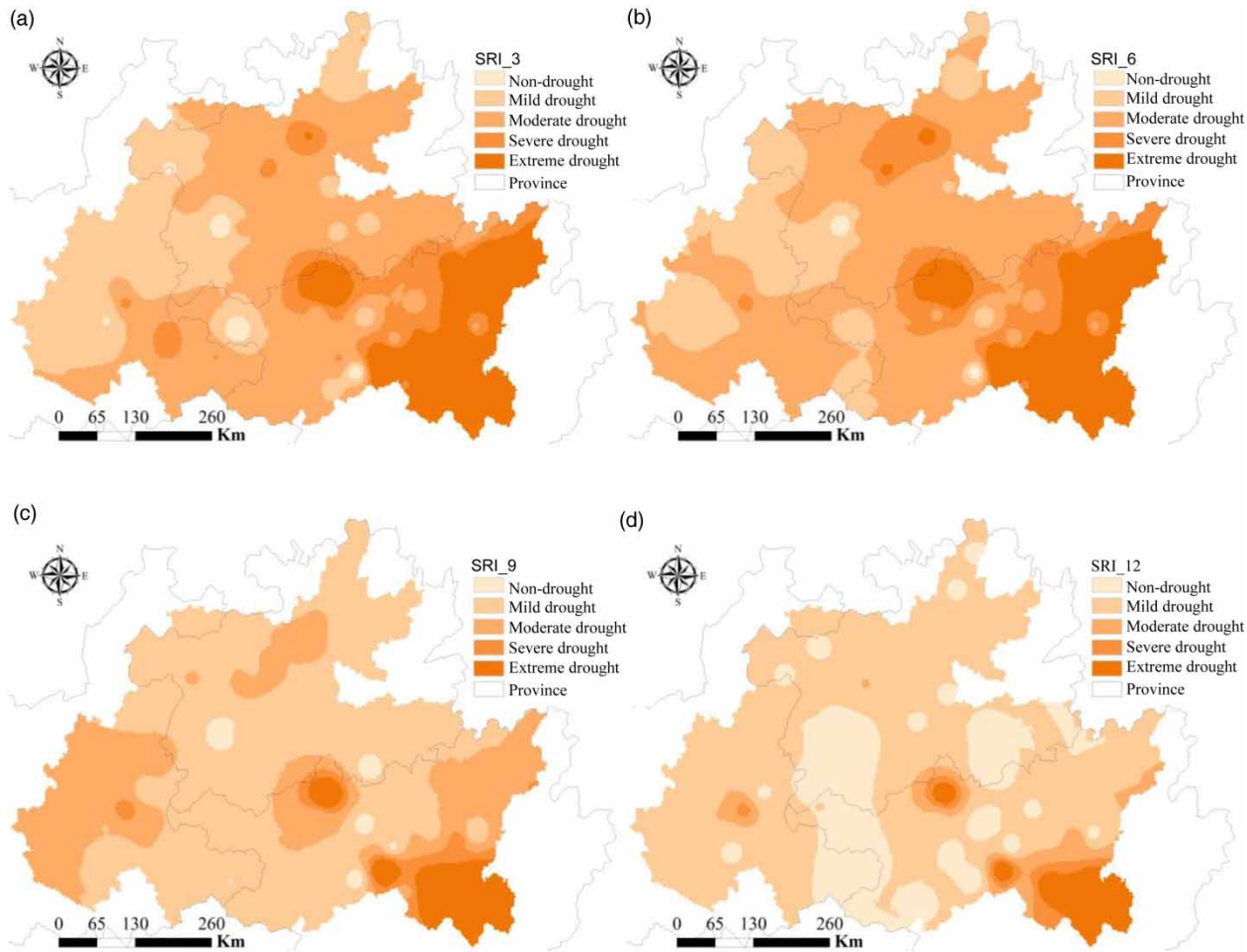

Figure 3 | The distribution characteristics of hydrologic drought grades in the *SRI_3* (a), *SRI_6* (b), *SRI_9* (c), and *SRI_12* (d).

also shown a decreasing trend with the increase of time scales. It further demonstrates that the runoff regulation effects or water storage functions of Karst drainage basins are more significant with the time scales increasing.

From the spatial distribution, (i) the hydrological drought intensity of the Karst drainage basins in South China is a gradually aggravating trend from the west to east parts and is showing a significant *north–south stripe* distribution at the *SRI_3* and *SRI_6* (Figure 3(a) and 3(b)). (ii) The mild, moderate, and severe or above hydrologic droughts are mainly distributed in the eastern, central, and western of research areas at the *SRI_3* and *SRI_6* with the area percentages of 28.75, 46.23 and 25.04%; and 20.51, 52.23 and 27.28%, respectively, and in the most part of the central, southwest, and southeast of research areas at the *SRI_12* (Figure 3(c)). (iii) Whether at the *SRI_3* and *SRI_6*, or at the *SRI_9* and *SRI_12*, the severe or above hydrologic droughts are found in the Zhijin Basin of Guizhou Province, the Yiguba Basin of Yunnan Province, the Tianzhu and Du'an Basin of Guangxi Province, while the mild or below hydrologic droughts in the Panjiangqiao Basin of Guizhou Province and the Fengyu Basin of Guangxi Province.

4.2.2. Analysis of hydrological drought characteristics based on different lithology-combined structures

As shown in Figure 4, (i) the moderate or below hydrological droughts ($-1.5 < SRI$) are observed in Classes I to V at the four types of time scales (*SRI_3*, *SRI_6*, *SRI_9*, and *SRI_12*). The severe or above hydrologic droughts ($SRI < -1.5$) are gradually decreased with the increase of time scales, especially the severe hydrologic droughts ($-2.0 < SRI < -1.5$) is shown a parallel distribution and rapid decline. (ii) For the *SRI_3* (Figure 4(a)), it is presented a *peak value* for the mild and extreme hydrologic droughts in Classes I, IV, and V, and a *low valley* phenomenon for the extreme hydrologic droughts in Class II and the mild hydrologic droughts in Class III, as well as a trend of first increase and then decrease for the moderate hydrologic droughts ($-1.5 < SRI < -1.0$) in Classes I to V. (iii) In terms of the *SRI_6* (Figure 4(b)), the *peak value* of mild hydrologic droughts is shown a *north shifting* phenomenon and that of extreme hydrologic droughts is shown a *south shifting* phenomenon. The distribution areas of moderate hydrologic drought ($-1.5 < SRI < -1.0$) in Classes I to V appear as a gradually decreasing trend and are obviously shown a *peak value* phenomenon in Class III. For the Classes I to V, the densities of moderate or below hydrological droughts are smaller with the density gradient changing slowly, and these of severe or above hydrologic droughts are larger with the density gradient changing rapidly. (iv) For the 9-month scale (*SRI_9*) (Figure 4(c)), the significant increasing trend and the obvious *peak-valley* alternating phenomena in Classes I to V are found for the distribution areas of mild hydrological droughts, the rapidly decreasing trend for these of severe or above hydrologic droughts, and the parallel distribution for these of moderate hydrological droughts. The mild hydrologic droughts are shown the *two peaks and one valley* in Class I, the *single-peak* distribution in Class V, and the *peak flattening* phenomenon in Class III, respectively. The severe or above hydrologic droughts are presented the *peak value* in Classes I, III, and IV, and the *low valley* in Classes II and V. The larger densities and density gradient changes rapidly are observed for the severe or above hydrological droughts in Classes I to V. (v) As shown in Figure 4(d) at the *SRI_12*, the distribution areas of mild hydrologic droughts in Classes I to V are accounted for a larger proportion, while those of severe or above hydrologic droughts in Class V has disappeared. There are still *two peaks and one valley* for the distribution regions of mild hydrologic droughts in Class I, the *single-peak* distribution for these of severe or above hydrologic droughts, and the *low valley* phenomenon in Class II. The *gradient distributions* obviously appeared for the hydrological droughts in Classes II to V, and the gradient changes of moderate or below hydrologic droughts are relatively slow, and these of severe or above hydrologic droughts are relatively steep.

4.3. Analysis on the driven mechanism of hydrologic drought in Karst Basins

4.3.1. Driven mechanism of single lithological type to hydrologic drought

Figure 5 shows that (i) the 11 kinds of watershed lithologies have produced some influences on hydrologic droughts, and these impacts are mainly concentrated in the mild, moderate, and severe hydrologic droughts at the *SRI_3* and *SRI_6* (Figure 5(a) and 5(b)), and in the moderate or below hydrologic droughts at the *SRI_9* and *SRI_12* (Figure 5(c) and 5(d)). (ii) For the 3-month scale (*SRI_3*) (Figure 5(a)), it mainly occurs the mild and moderate hydrologic droughts in the Pt to K distribution regions. Especially the occurrence probabilities are the largest (0.5–0.6) in the C, P, and T distribution regions, followed by in the Z, ε, O, J, and K distribution regions with the occurrence probabilities 0.35–0.45, while the smallest (0.2–0.3) in the Pt, S, and D distribution regions. (iii) For the 3-month scale (*SRI_3*) (Figure 5(a)), there are mainly the mild and moderate hydrologic droughts in the Pt to K distribution areas. Especially the occurring probability is the largest (0.5–0.6) in the C, P, and T distribution areas, followed by in the Z, ε, O, J, and K distribution areas with the occurring probabilities 0.35–0.45, while the smallest (0.2–0.3) in the Pt, S, and D distribution areas. The largest (0.75) is the occurring

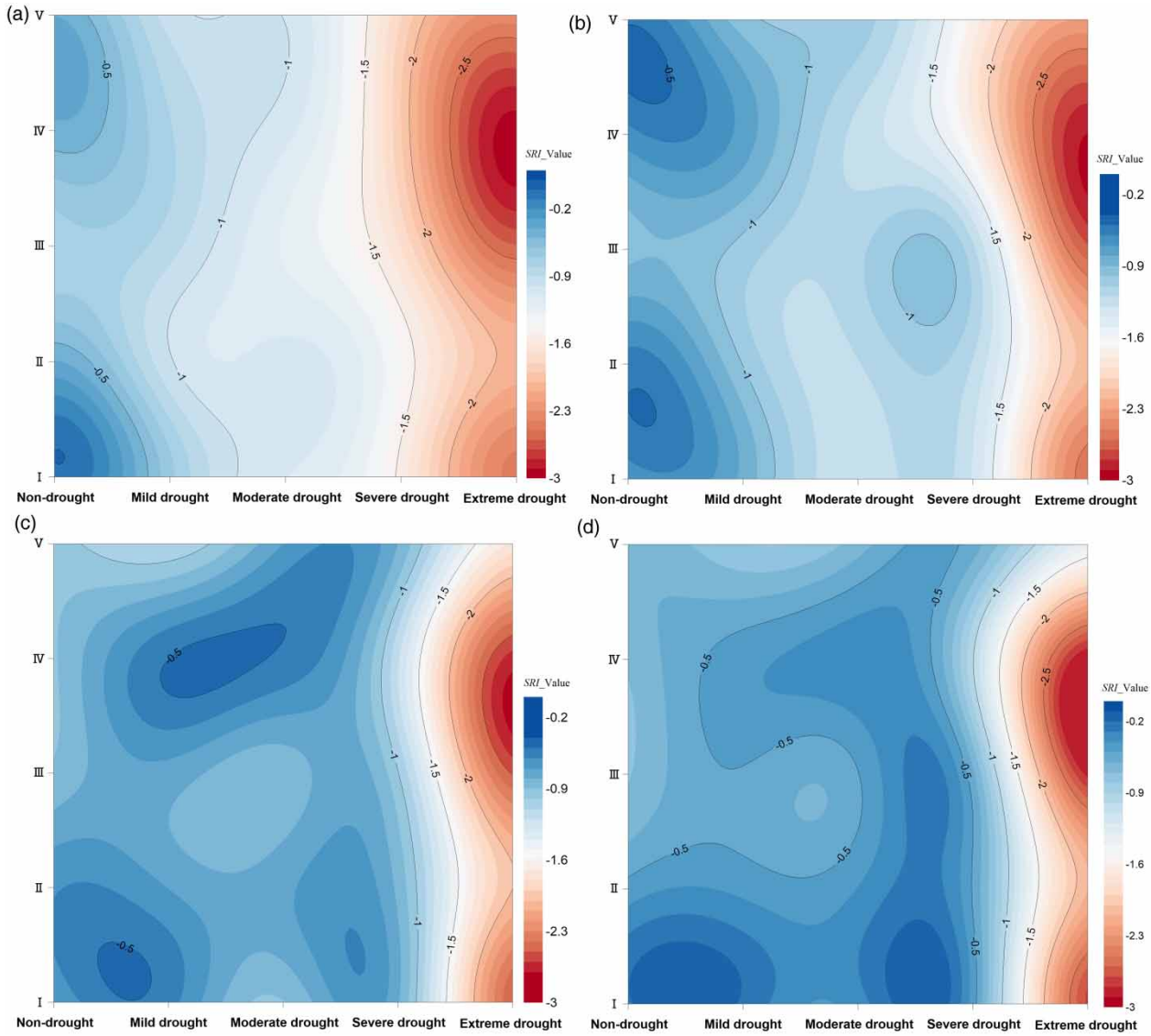

Figure 4 | The distribution characteristics of hydrological drought probabilities in Classes I to V basins in the *SRI_3* (a), *SRI_6* (b), *SRI_9* (c), and *SRI_12* (d).

probabilities of severe and extreme hydrological droughts in the Pt, followed by in the S, D, and J distribution regions (0.15–0.35). (iv) It mainly occurs the moderate hydrologic droughts at the *SRI_6* (Figure 5(b)). Especially the largest is the occurring probabilities in the C, P, T, and K distribution regions, followed by in the Z, ε, O, S, D, and J distribution regions with the occurring probability 0.35–0.4, the smallest (0.2) in the Pt distribution region. The largest probability (0.75) of severe or above hydrologic droughts is observed in the Pt distribution region, the smallest (0.1–0.2) in the rest of the lithologic distribution regions. The occurrence probability of the severe or above hydrologic droughts is the largest (0.75) in the Pt distribution area, while the smallest (0.1–0.2) in the rest of the lithologies. (v) For the 9-month and 12-month scales (*SRI_9*, *SRI_12*) shown in Figure 5(c) and 5(d), the mild hydrologic droughts are mainly presented in the Pt to K distribution regions. Among them, the occurrence probability of mild hydrologic droughts is the largest (0.55–0.8) in the C to K and Z distribution regions at the *SRI_12*, followed by in the Z to O distributions (0.3–0.6), while the smallest (0.2–0.3) in the S, D, and Pt distribution regions. For the C to K distribution regions, the mild to moderate hydrologic droughts are shown a slower change and smaller gradient at the *SRI_9*, a faster change and larger gradient at the *SRI_12*, and the severe and extreme hydrologic droughts have basically not happened. There are the slowest change and smallest gradient for the mild

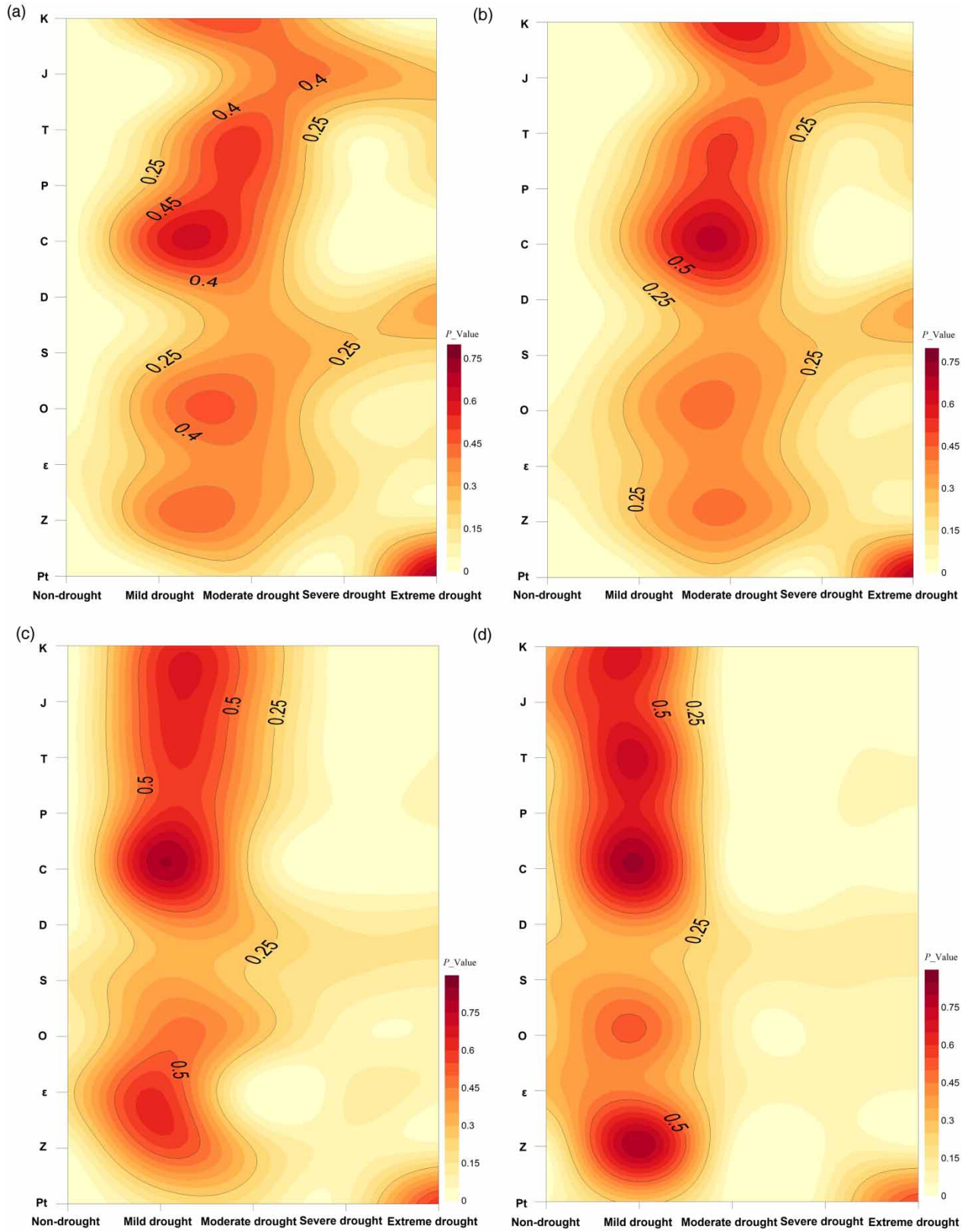

Figure 5 | The driven mechanism of hydrologic drought by single lithologic type in the *SRI_3* (a), *SRI_6* (b), *SRI_9* (c), and *SRI_12* (d).

to moderate hydrologic droughts in the S and D distribution regions, and the severe and extreme hydrologic droughts have a certain occurrence probability (0.15). A slower change and smaller gradient are found for the mild to moderate hydrologic droughts in the Pt to O distribution regions, however the severe hydrological droughts have disappeared, and extreme hydrological droughts have a larger occurring probability (0.55).

4.3.2. Driven mechanism of lithology-combined structures to hydrologic drought

It is known from the lithology-combined structures (Figure 6) that (i) the five kinds of structures have all produced the influences on the hydrological droughts. Among them, the impacts are mainly concentrated in the mild and moderate hydrologic droughts at the *SRI_3* and *SRI_6*, the mild or below hydrologic droughts at the *SRI_9* and *SRI_12*. This indicates that the response of Karst basins to atmospheric precipitation is shown a lag, and the lagged effects of different lithology-combined structures have great differences. It shows more and more significant with the increase of time scales. (ii) For the 3-month scale (*SRI_3*) shown in Figure 6(a), the mild and moderate hydrologic droughts are observed in Classes I to V, especially

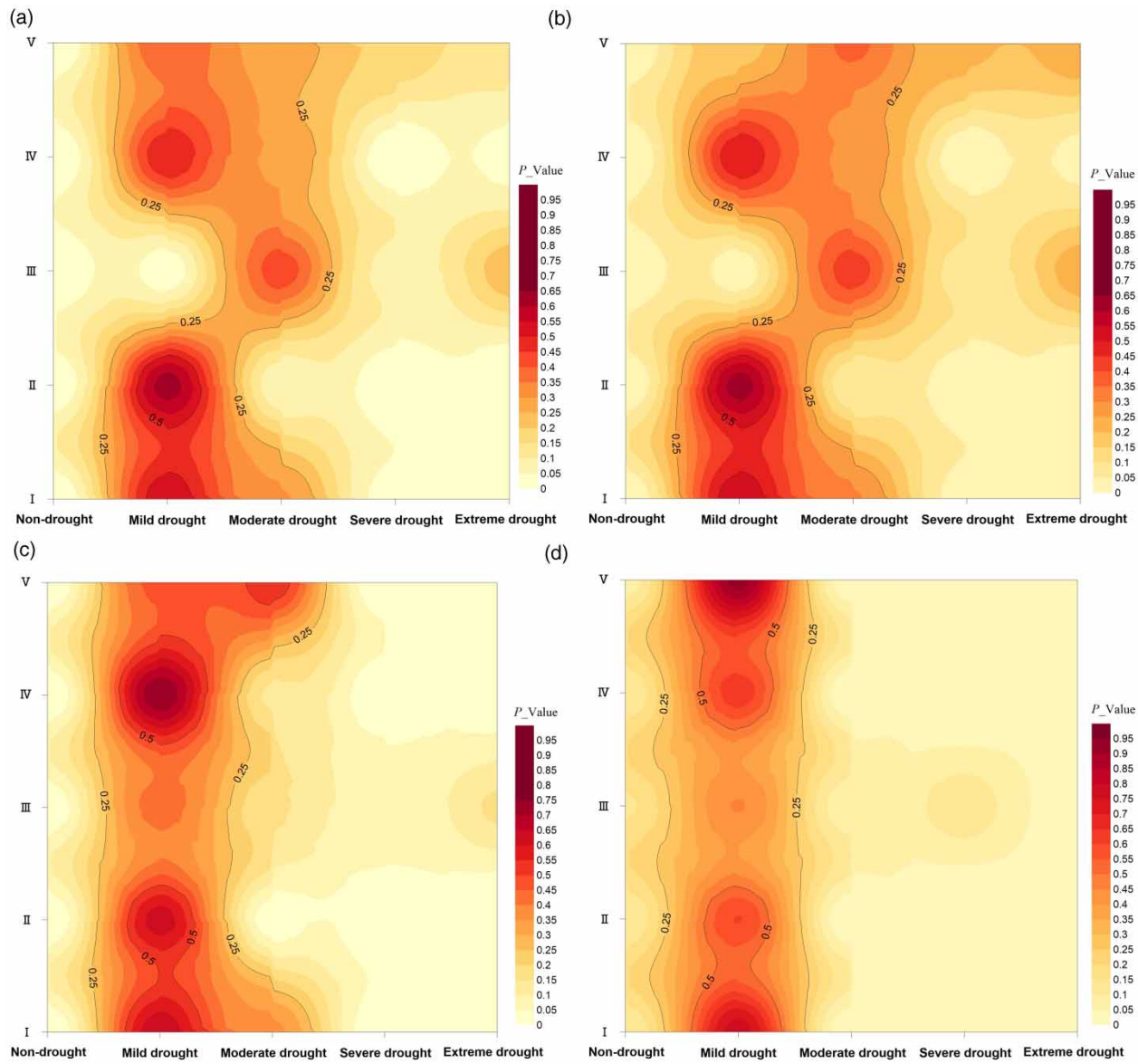

Figure 6 | The driven mechanism of hydrologic drought by lithology-combined structures in the *SRI_3* (a), *SRI_6* (b), *SRI_9* (c), and *SRI_12* (d).

with the largest probability (0.6) in Class II, followed by in Classes I and IV with the occurrence probability 0.5. It hardly occurs the mild hydrologic droughts in Class III, but occurs the moderate hydrologic droughts with the occurring probability 0.4. The severe and extreme hydrologic droughts hardly happen in Classes I, II, and IV, and show the occurrence probabilities of 0.2–0.3 in Classes III and V. The mild to extreme hydrologic droughts are shown the larger gradient and faster change in Classes I and II, and the smaller gradient and slower change in Classes IV and V, as well as a certain fluctuation characteristics in Class III. (iii) For 6-month scale (*SRI_6*), it mainly occurs the mild hydrologic droughts in Classes I, II, and IV with the occurring probabilities of 0.5–0.6 (Figure 6(b)), and the moderate hydrologic drought in Classes III and V with the occurring probabilities of 0.35–0.4. Similar to the *SRI_3*, the severe and extreme hydrologic droughts do not basically happen at the *SRI_6* in Classes I, II, and IV, and show a certain occurring probabilities of 0.05–0.2 in Classes III and IV. The occurrence probability of mild hydrologic droughts is gradually decreasing at the *SRI_6* in Class V, and that of moderate hydrologic droughts is just the opposite. (iv) Compared with the *SRI_3* and *SRI_6*, it mainly occurs the mild hydrologic drought at the *SRI_9* and *SRI_12* (Figure 6(c) and 6(d)). Especially the highest (0.45–0.9) is the occurring probability of mild hydrologic droughts in Class V, followed by in Classes I, II, and IV (0.6–0.75), and the smallest (0.4–0.45) in Class III. The mild to extreme hydrologic droughts in Classes I to V are presented the slower change and smaller gradient at the *SRI_9*, and the faster change and larger gradient at the *SRI_12*. It hardly occurs the severe or above hydrologic droughts at the *SRI_9* and the moderate or above hydrologic droughts at the *SRI_12*. From the Classes I to IV, the mild hydrological droughts are shown the larger distribution areas with a higher probability at the *SRI_9*, and the smaller distribution areas with a lower probability at the *SRI_12*. Especially in Class V, the mild and moderate hydrologic droughts at the *SRI_9* are mainly appeared the mild hydrologic droughts at the *SRI_12*.

5. DISCUSSION

Attributed to the soluble aqueous medium under the differential erosion or solution effects of soluble water, many sizes of spaces are formed in Karst drainage basins, which provide some places for atmospheric precipitation lag flow on the surface and underground, and makes the basins have a certain storage capacity. This paper justly attempts to explore the watershed storage capacities in terms of lithologic types and spatial coupling structures, and to reveal the mechanism of hydrological droughts. According to this research purpose, this paper firstly selected 55 samples in Karst distribution areas of South China, and collected monthly runoff data from 1970 to 2013, and extracted the basin lithology data. Secondly, the temporal and spatial evolution characteristics of hydrological droughts in Karst drainage basins of South China were analyzed using the *SRI*, and the mechanism of hydrological droughts were discussed employing the cluster statistical method and Bayesian formula of probability theory in terms of single lithology and spatial coupling of basin lithologies. Therefore, this study has realized the initial research assumption, and these research results have good applicability for Karst drought monitoring and prediction. However, this study mainly considered the Karst research areas, and the research results have certain limitations for the application in Non-Karst areas.

The double aqueous medium and dual water system structures on the surface and underground are developed in Karst drought basins compared with the normal basins, which results in the significant response of watershed runoff to atmospheric precipitation at different time scales (Wang *et al.* 2002; He *et al.* 2015a, 2015b). This study demonstrates that the hydrological droughts are relatively serious at the 3-, 6-, and 9-month scales, and a relatively lighter at the *SRI_12*. The occurrence level of hydrological droughts is mainly shown the extreme hydrological drought (6.28%) < severe hydrological drought (6.52%) < non-drought (7.15%) < moderate hydrological drought (32.8%) < mild hydrological drought (47.25%). It proves that Karst drain basins have a stronger water storage function, and their water storage capacities become more and more significant with the increase of time scales. Meanwhile, many types of lithologies, impure textures, and complex structures are observed in Karst drainage basins, where are developed the different sizes of water-stored spaces under the differential erosion or solution effects of soluble water, such as the solution gap, solution hole, and pipeline, as well as the underground cave and underground corridor. As a result, the response of different lithologic combination structures to atmospheric precipitation is significantly different (He & Chen 2013; He *et al.* 2013, 2014; López-Moreno *et al.* 2013). This study indicates that in terms of lithology combination structures, the hydrological drought is the most serious in Class V with the drought area 95.94%, followed by in Classes IV, III, and I with the drought areas of 94.41, 92.25, and 91.95%, respectively, and the relatively lighter (90.95%) in Class II. The severity of hydrological droughts is the Classes II and III (91.79%) < Classes I and IV (92.15%) < Class V (95.94%) in terms of the combination types of watershed lithologies, and the Classes I and III (90%) <

Classes II and IV (92.2%) < Class V (95.94%) in terms of Karst lithologies. These conclusions are supported by He *et al.* (2015b).

The watershed lithologies are the material bases controlling the geomorphic development and soil formation. The different watershed lithologies are shown the different resistance abilities because their lithologic compositions, particle sizes, and composite structures have the larger differences, which promotes or inhibits the formation of water-stored spaces in Karst drainage basins. Therefore, the driving capacity of different watershed lithology types and spatial coupling structures to hydrological droughts have significant differences. This study shows that the driving probability of single lithology to hydrologic droughts is the Pt (0.15) < J, D and S (0.3) < T, O, and ε (0.4) < K (0.45) < P and Z (0.5) < C (0.6) in the distribution areas of mild hydrologic droughts, the Pt (0.15) < ε (0.2) < Z (0.25) < J, D, S, O, P, and C (0.3) < T (0.35) < K (0.4) in the distribution areas of moderate hydrologic droughts, the C (0) < Pt, P, and T (0.05) < Z, O, and K (0.1) < ε < D (0.15) < J and S (0.2) in the distribution areas of severe hydrologic droughts, and the C (0) < O, K, and ε (0.05) < P, T, and Z (0.1) < J and S (0.15) < D (0.2) < Pt (0.6) in the distribution areas of extreme hydrologic droughts. On the whole, the O, C, and T (0.15) < Pt, Z, ε, D, and P (0.2) < S, J, and K (0.25). This may be that the O, C, and T, dominated by the soluble calcite, are easy to be formed the different sizes of water-stored spaces under the differential dissolution or erosion effects of soluble water, which enhances the watershed storage capacity and inhibits the occurrence of hydrologic droughts in a certain extent. On the contrary, the S, J, and K, dominated by the insoluble quartz, feldspar, and kaolinite, are difficult to be formed the water-stored spaces, which weakens the watershed storage capacity and promotes the occurrence of hydrologic droughts. Thus, this study shows that the driving probability of hydrological droughts is the Class II (0.15) < Class III (0.19) < Class IV (0.2) < Class I (0.22) < Class V (0.25) in terms of lithology combination structures, the Classes II and III (0.17) < Classes I and IV (0.22) < Class V (0.25) in terms of the composite types of watershed lithologies, and the Classes I and III (0.18) < Classes II and IV (0.2) < Class V (0.25) in terms of Karst lithologies. It means that under the differential erosion or solution effects of soluble water, the water-stored spaces formed in Karst Basins is the most, followed by in the Semi-Karst Basins, the least in the Non-Karst Basins. This further proves that the watershed storage capacity is the Non-Karst Basin (V) < Semi-Karst Basin (II and IV) < Karst Basin (I and III).

To sum up, the watershed runoff and atmospheric precipitation do not happen at the same time and have a certain lag in time. Its lag time and intensity are greatly affected by the watershed storage capacity. The Karst drainage basin has a certain storage capacity attributed to the Karst lithology with the solubility under the differential dissolution or erosion effects of soluble water. This study proves that there are the most water-stored spaces or the strongest storage capacity in the Limestone Karst Basin (II and III), followed by in the Dolomite Karst Basin (I and IV), the least water-stored spaces or the weakest storage capacity in the Non-Karst Basin (V). Similarly, the most water-stored spaces or the strongest storage capacity are found in the Karst Basin (I and III), followed by in the Semi-Karst Basin (II and IV), the least water-stored spaces or the weakest storage capacity in the Non-Karst Basin (V). Therefore, this study provides a technical guidance for Karst drought monitoring and warning and a theoretical basis for drought relief, and effectively promotes the development of hydrogeology.

6. CONCLUSION

The watershed lithology is an important component of basin underlying surfaces. The development of the landform and river system and the formation of watershed-stored spaces controlled by the watershed lithologic types and structures will promote or inhibit the occurrence of hydrological droughts. As analyzed above, the driven mechanisms of Karst lithologies and their composite structures to hydrological droughts can be summarized as follows:

1. There is few single lithologic type in Karst drainage basins, and two or more than lithologic types mixed. The basins could be divided into five types according to watershed lithology-combined structures, namely the Dolomite Karst Basin (I), Limestone Semi-Karst Basin (II), Limestone Karst Basin (III), Dolomite Semi-Karst Basin (IV), and Non-Karst Basin (V), respectively.
2. The hydrological droughts of Karst drainage basins in South China are widely distributed, and the drought intensities are gradually decreasing with the time scales increasing. Among them, the hydrological droughts are relatively serious at the *SRI_3*, *SRI_6*, and *SRI_9*, and relatively lighter at the *SRI_12*. It indicates that the effects of Karst drainage basins on the runoff regulations are more and more significant with the increase of time scales, and hydrologic drought intensities are more and more lighter. Meanwhile, the hydrological droughts from the west to east parts, South China are gradually aggravating with the *north–south stripe* distribution that is the most significant at the *SRI_3* and *SRI_6*.

3. The driven effects of Karst basins on hydrologic droughts are closely related to the solubility of lithology. Hence, the occurrence probability of hydrological droughts is the O, C, and T (0.15) < Pt, Z, ε, D, and P (0.2) < S, J, and K (0.25). The driven effects of different types of basins on hydrologic droughts have significant differences due to the different lithologic types and spatial coupling structures. Among them, it mainly occurs the mild and moderate hydrologic droughts at the *SRI_3* and *SRI_6*, and the mild or below hydrologic droughts at the *SRI_9* and *SRI_12*. The occurrence probability of hydrological droughts is the Limestone Semi-Karst Basin (II, 0.15) < Limestone Karst Basin (III, 0.19) < Dolomite Semi-Karst Basin (IV, 0.2) < Dolomite Karst Basin (I, 0.22) < Non-Karst Basin (V, 0.25) in terms of basin types, the Limestone Karst Basin (II, III, 0.17) < Dolomite Karst Basin (I, IV, 0.22) < Non-Karst Basin (V, 0.25) in terms of composite structures of basin lithologies, and the Karst Basin (I, III, 0.18) < Semi-Karst Basin (II, IV, 0.2) < Non-Karst Basin (V, 0.25) in terms of Karst lithologies, respectively.

ACKNOWLEDGEMENTS

This study was supported by the Natural Science Foundation of China (41471032; u1612441); the Natural and Scientific Research Fund of Guizhou Water Resources Department (KT201402); the Natural and Scientific Fund of Guizhou Science and Technology Agency (QKH J [2010] No. 2026, QKH J [2013] No. 2208); 2015 Doctor Scientific Research Startup Project of Guizhou Normal University.

DATA AVAILABILITY STATEMENT

All relevant data are included in the paper or its Supplementary Information.

REFERENCES

Abebe, A. & Foerch, G. 2008 Stochastic simulation of the severity of hydrological drought. *Water and Environment Journal* **22** (1), 2–10. https://doi.org/10.1111/j.1747-6593.2007.00080.x.

Ding, Y. B., Xu, J. T. & Wang, X. W. 2021 Propagation of meteorological to hydrological drought for different climate regions in China. *Journal of Environmental Management* **283**, 1–12.

Feng, G. 1993 An analysis of frequency of critical drought duration in independent hydrologic series. *Agricultural Research in the Arid Areas* **11** (3), 60–68.

Feng, G. 1994 A study on probability distribution of critical hydrologic drought durations using the methods of analytic and simulation. *Acta Geographica Sinica* **49** (5), 457–468.

Feng, G. 1995 An analysis frequency of critical hydrologic drought duration. *Shuili Xuebao* **6**, 37–41. doi:10.13243/j.cnki.slxb.1995.06.006.

Feng, P. & Jia, H. 1997 Investigation on forecasting model of hydrological drought in water supply systems. *Journal of Tianjin University* **30** (3), 337–342.

Feng, P. & Wang, R. 1997 Investigation on the time fractal of hydrologic drought. *Water Conservancy and Hydropower Technology* **11**, 48–51.

Firoz, A. B. M., Nauditt, A. & Fink, M. 2018 Quantifying human impacts on hydrological drought using a combined modelling approach in a tropical river basin in central Vietnam. *Hydrology and Earth System Sciences* **22**, 547–565. https://doi.org/10.5194/hess-22-547-2018.

Fleig, A., Tallaksen, L. & Hisdal, H. 2011 Regional hydrological drought in north-western Europe: linking a new Regional Drought Area Index with weather types. *Hydrological Processes* **25**, 1163–1179. https://doi.org/10.1002/hyp.7644.

Guven, O. 1983 A simplified semiempirical approach to probabilities of extreme hydrologic droughts. *Water Resource Research* **19** (2), 441–453. https://doi.org/10.1029/WR019i002p00441.

Hao, Z., Hao, F., Singh, V., Sun, A. Y. & Xia, Y. 2016 Probabilistic prediction of hydrologic drought using a conditional probability approach based on the meta-Gaussian model. *Journal of Hydrology* **542**, 772–780. https://doi.org/10.1016/j.jhydrol.2016.09.048H.

He, Z. & Chen, X. 2013 The hydrological drought simulating in Karst Basin based on coupled soil factors–taking Guizhou Province as a case. *Scientia Geographica Sinica* **33** (6), 724–734.

He, Z., Chen, X., Liang, H., Huang, F. & Zhao, F. 2012 Quantitative remote sensing monitoring and analysis of Karst water resources based on NDVI – taking Guizhou Province as a case. *Research of Soil and Water Conservation* **19** (3), 161–165.

He, Z., Chen, X. & Liang, H. 2013 The hydrological drought analysis of the Karst Basin based on the soil systematic structure–taking Guizhou Province as a case. *Journal of Natural Resource* **28** (10), 1731–1741. https://doi.org/10.11849/zrzyxb.2013.10.008.

He, Z., Chen, X. & Liang, H. 2014 Study on spatial pattern of land-using types and hydrologic droughts for typical Karst Basin of Guizhou Province. *Journal of China Hydrology* **34** (1), 20–25.

He, F., Hu, C., Wang, J. & Wang, Y. 2015a Analysis of meteorological and hydrological drought in the Yellow River Basin during the past 50 years based on SPI and SDI. *Geography and Geo-Information Science* **31** (3), 69–75.

He, Z., Chen, X. & Liang, H. 2015b Studies on the mechanism of watershed hydrologic droughts based on the combined structure of typical Karst lithologys. *Chinese Journal of Geology* **50** (1), 340–353. https://doi.org/10.3969/j.issn.0563-5020.2015.01.023.

He, Z., Ling, H., Yang, Z., Huang, F. & Zeng, X. 2018a Temporal–spatial evolution of the hydrologic drought characteristics of the karst drainage basins in South China. *International Journal of Applied Earth Observation and Geoinformation* **64** (2), 22–30. http://dx.doi.org/10.1016/j.jag.2017.08.010.

He, Z., Ling, H. & Yang, Z., Huang, F. & Zeng, X. 2018b Water system characteristics of Karst River Basins in South China and their driving mechanisms of hydrological drought. *Natural Hazards* **92**, 1155–1178. https://doi.org/10.1007/s11069-018-3275-2.

Hisdal, H. & Tallaksen, L. M. 2003 Estimation of regional meteorological and hydrological drought characteristics: a case study for Denmark. *Journal of Hydrology* **281** (3), 230–247. https://doi.org/10.1016/S0022-1694(03)00233-6.

Jehanzaib, M., Shah, S. A. & Yoo, J. 2020 Investigating the impacts of climate change and human activities on hydrological drought using non-stationary approaches. *Journal of Hydrology* **588** (2020), 125052. https://doi.org/10.1016/j.jhydrol.2020.125052.

Jiao, S. & Liang, H. 2002 The research on the relationship between drainage basins' landforms and its lithologic features in Karst region—a case study in Guizhou Province. *Carsologica Sinica* **21** (2), 95–100.

Kang, Q. & Guo, F. 1991 A study on the relation of hydrologic drought and soil water movement. *Journal of North China Institute of Water Conservancy and Hydroelectric Power* **2**, 11–16.

Kim, T. W. & Valdés, J. B. 2006 Nonparametric approach for bivariate drought characterization using Palmer Drought Index. *Journal of Hydrologic Engineering* **11** (2), 134–143.

Leng, G. Y., Tang, Q. H. & Scott, R. B. 2015 Climate change impacts on meteorological, agricultural and hydrological droughts in China. *Global and Planetary Change* **126**, 23–34. http://dx.doi.org/10.1016/j.gloplacha.2015.01.003.

Li, Y., He, J. & Li, X. 2016 Hydrological and meteorological droughts in the Red River Basin of Yunnan Province based on SPEI and SDI indices. *Progress in Geography* **35** (6), 758–767. https://doi.org/H10.18306/dlkxjz.2016.06.009.

Liang, H. 1995 Effect analysis of hydrogeomorphologic making flood peak in Karst drainage basin. *Carsologica Sinica* **14** (3), 223–229.

Liang, H. 1997 Preliminary study on the characteristics of flood discharge and low flow influenced by the scale of Karst drainage basin – exampled by the rivers in Guizhou Province. *Carsologica Sinica* **16** (2), 121–129.

Liang, H. & Wang, J. 1998 A relative analysis between the lithological features and characteristics of flood discharge and low flow in Karst district – case study of the rivers, Guizhou Province. *Carsologica Sinica* **17** (1), 67–73.

Liao, J., Wang, W. & Ding, J. 2007 Comprehensive assessment of water quality on main rivers in Sichuan by Bayes method. *Journal of Sichuan Normal University (Natural Science)* **30** (4), 519–522.

Liu, L., Yang, H., Christopher, N., Yong, B., Shafer, M. A., Riley, R. & Hocker, J. E. 2012 Hydro-climatological drought analyses and projections using meteorological and hydrological drought indices: a case study in Blue River Basin, Oklahoma. *Water Resources Management* **26**, 2761–2779. https://doi.org/H10.1007/s11269-012-0044-y.

Liu, X. L., Xu, X. H. & Yu, M. X. 2016 Hydrological drought forecasting and assessment based on the Standardized Stream Index in the Southwest China. *Procedia Engineering* **154**, 733–737.

López-Moreno, J. I., Vicente-Serrano, S. M. & Zabalza, J. 2013 Hydrological response to climate variability at different time scales: a study in the Ebro Basin. *Journal of Hydrology* **477**, 175–188. http://dx.doi.org/10.1016/j.jhydrol.2012.11.028.

Ma, M. & Song, S. 2010 Elliptical copulas for drought characteristics analysis of Xi'an gauging station. *Journal of China Hydrology* **30** (4), 36–42.

Modarres, R. Z. & Sarhadi, A. 2010 Frequency distribution of extreme hydrologic drought of southeastern semiarid region, Iran. *Journal of Hydrologic Engineering* **15** (4), 255–264. http://dx.doi.org/1084-0699/2010/4-255–264/$25.00.

Mondal, A. & Mujumdar, P. 2015 Return levels of hydrologic droughts under climate change. *Advances in Water Resources* **75**, 67–79. https://doi.org/10.1016/j.advwatres.2014.11.005.

Nalbantis, I. & Tsakiris, G. 2009 Assessment of hydrological drought revisited. *Water Resources Management* **23** (5), 881–897. https://doi.org/10.1007/s11269-008-9305-1.

Nyabeze, W. R. 2004 Estimating and interpreting hydrological drought indices using a selected catchment in Zimbabwe. *Physics and Chemistry of the Earth* **29**, 1173–1180. https://doi.org/10.1016/j.pce.2004.09.018.

Panu, U. S. & Sharma, T. C. 2009 Analysis of annual hydrological droughts: the case of northwest Ontario, Canada. *Hydrological Sciences Journal* **54** (1), 29–42.

Ren, L., Shen, H., Yuan, F. & Zhao, C. 2016 Hydrological drought characteristics in the Weihe catchment in a changing environment. *Advances in Water Science* **27** (4), 492–500. https://doi.org/H10.14042/j.cnki.32.1309.2016.04.002.

Rudd, A. C., Bell, V. A. & Kay, A. L. 2017 National-scale analysis of simulated hydrological droughts (1891–2015). *Journal of Hydrology* **550**, 368–385. http://dx.doi.org/10.1016/j.jhydrol.2017.05.018.

Ryu, J. H., Svoboda, M. D. & Lenters, J. D. 2010 Potential extents for ENSO-driven hydrologic drought forecasts in the United States. *Climatic Change* **101**, 575–597. https://doi.org/10.1007/s10584-009-9705-0.

Seibert, M., Merz, B. & Apel, H. 2017 Seasonal forecasting of hydrological drought in the Limpopo Basin: a comparison of statistical methods. *Hydrology and Earth System Sciences* **21**, 1611–1629. https://doi.org/10.5194/hess-21-1611-2017.

Sen, Z. 1977 Run-sums of annual flow series. *Journal of Hydrology* **35** (3), 311–324. https://doi.org/10.1016/0022-1694(77)90009-9.

Sen, Z. 1990 Critical drought analysis by second-order Markov chain. *Journal of Hydrology* **120**, 183–202. https://doi.org/10.1016/0022-1694(90)90149-R.

Sen, Z. 1991 On the probability of the longest run length in an independent series. *Journal of Hydrology* **125**, 37–46. https://doi.org/10.1016/0022-1694(91)90082-S.

Sharma, T. C. 1998 An analysis of non-normal Markovian extremal droughts. *Hydrology Process* **12**, 597–611.

Swetalina, N. & Thomas, T. 2016 Evaluation of hydrological drought characteristics for Bearma basin in Bundelkhand region of Central India. *Procedia Technology* **24**, 85–92.

Tabari, H., Nikbakht, J. & Talaee, P. H. 2013 Hydrological drought assessment in northwestern Iran based on Streamflow Drought Index (SDI). *Water Resources Management* **27**, 137–151. https://doi.org/10.1007/s11269-012-0173-3.

Tallaksen, L. M., Hisdal, H. & Van Lanen, H. A. J. 2009 Space-time modeling of catchment scale drought characteristics. *Journal of Hydrology* **375**, 363–372. https://doi.org/10.1016/j.jhydrol.2009.06.032.

Tigkas, D., Vangelis, H. & Tsakiris, G. 2012 Drought and climatic change impact on streamflow in small watersheds. *Science of the Total Environment* **440**, 33–41. https://doi.org/10.1016/j.scitotenv.2012.08.035.

Tsakiris, G., Pangalou, D. & Vangelis, H. 2007 Regional drought assessment based on the Reconnaissance Drought Index (RDI). *Water Resources Management* **21**, 821–833. https://doi.org/10.1007/s11269-006-9105-4.

Tu, X., Chen, X., Zhao, Y., Du, Y., Ma, M. & Li, K. 2016 Responses of hydrologic drought properties and water shortage under changing environments in Dongjiang River Basin. *Advances in Water Science* **27** (6), 810–821. https://doi.org/10.14042/j.cnki.32.1309.2016.06.003.

Van Loon, A. F. & Laaha, G. 2015 Hydrological drought severity explained by climate and catchment characteristics. *Journal of Hydrology* **526**, 3–14. https://doi.org/10.1016/j.jhydrol.2014.10.059.

Van Loon, A. F. & Van Lanen, A. J. 2012 A process-based typology of hydrological drought. *Hydrology and Earth System Sciences* **16**, 1915–1946. https://doi.org/H10.5194/hessd-8-11413-2011.

Vasiliades, L. & Loukas, A. 2009 Hydrological response to meteorological drought using the Palmer drought indices in Thessaly, Greece. *Desalination* **237**, 3–21. https://doi.org/10.1016/j.desal.2007.12.019.

Vazifehkhah, S. & Kahya, E. 2018 Hydrological drought associations with extreme phases of the North Atlantic and Arctic Oscillations over Turkey and northern Iran. *International Journal of Climatology* **38**, 4459–4475. https://doi.org/10.1002/joc.5680.

Wang, Z., Liang, H. & Yang, M. 2002 Analysis of the impact of different landform types on low flow modulus in karst regions: a case study of rivers in Guizhou Province. *Geographical Research* **21** (4), 441–448.

Wen, L., Rogers, K., Ling, J. & Saintilan, N. 2011 The impacts of river regulation and water diversion on the hydrological drought characteristics in the Lower Murrumbidgee River, Australia. *Journal of Hydrology* **405** (3), 382–391.

Wu, J., Chen, X., Gao, L. & Lin, Z. 2016 Construction and recognition of regional hydrological drought index based on standardized runoff index. *Mountain Research* **34** (3), 282–289. https://doi.org/10.16089/j.cnki.1008-2786.000129.

Xu, Y., Zhang, Q. & Lou, Z. 2010 Joint probability analysis of drought duration and severity based oil copula approach. *Journal of Tianjin University* **43** (10), 928–932.

Yan, B., Guo, S. & Xiao, Y. 2007 Analysis on drought characteristics based on bivariate joint distribution. *Arid Zone Research* **24** (4), 537–542.

Yang, P., Xia, J., Zhang, Y. Y. & Zhan, C. 2021 Quantitative study on characteristics of hydrological drought in arid area of Northwest China under changing environment. *Journal of Hydrology* **597**, 1–12. https://doi.org/10.1016/j.jhydrol.2021.126343.

Yevjevich, V. 1967 *An Objective Approach to Definition and Investigations of Continental Hydrologic Droughts*. Colorado State University. https://doi.org/10.1016/0022-1694(69)90110-3.

Zhai, J., Jiang, G., Pei, Y., Zhao, Y. & Xiao, W. 2015 Hydrologic drought assessment in the river basin based on Standard Water Resources Index (SWRI): a case study on the Northern Haihe River. *Shuili Xuebao* **46** (6), 687–698. https://doi.org/H10.13243/j.cnki.slxb.20140844.

Zhang, Y. H., Xiang, L., Sun, Q. & Chen, Q. 2016 Bayesian probabilistic forecasting of seasonal hydrological drought based on copula function. *Scientia Geographica Sinica* **36** (9), 1437–1444. doi:10.13249/j.cnki.sgs.2016.09.017.

Zhao, X. & Zhao, R. 2016 Applicability of the hydrologic drought index in the upper Fenhe River. *Advances in Water Science* **27** (4), 512–519. https://doi.org/H10.14042/j.cnki.32.1309.2016.04.004.

Zhou, Y., Yuan, X. & Jin, J. 2011 Regional hydrological drought frequency based on copulas. *Scientia Geographica Sinica* **31** (11), 1383–1388.

Zhou, Z., Shi, H. & Fu, Q. 2020 Characteristics of propagation from meteorological drought to hydrological drought in the Pearl River Basin. *Journal of Geophysical Research: Atmospheres*, 1–20. https://doi.org/10.1029/2020JD033959.

First received 25 April 2021; accepted in revised form 13 September 2021. Available online 30 September 2021